Magnetism in Solids

Mössbauer and Density Functional Studies of Ferrimagnetic Fe_3Se_4

Yang-Ki Hong[1], Jihoon Park[1,2], Hang Nam Ok[3], Minyeong Choi[1,4], Md Abdul Wahed[5], Myung-Hwa Jung[6], and Chang-Dong Yeo[5]

[1]*Department of Electrical and Computer Engineering and Materials Science, The University of Alabama, Tuscaloosa, AL 35487, USA*
[2]*Korea Institute of Materials Science, Changwon 51508, South Korea*
[3]*Department of Physics, Yonsei University, Seoul 03722, South Korea*
[4]*R&D Division, Hyundai Motor Company, NamYang 18280, South Korea*
[5]*Department of Mechanical Engineering, Texas Tech University, Lubbock, TX 79409, USA*
[6]*Department of Physics, Sogang University, Seoul 04107, South Korea*

Received 15 Aug 2024, revised 25 Sep 2024, accepted 26 Sep 2024, published 14 Oct 2024, current version 14 Nov 2024.

Abstract—Monoclinic Fe_3Se_4 was synthesized using a ceramic method. Mössbauer spectroscopy and density functional theory were used to investigate the physical origins of its ferrimagnetism and high coercivity. At 78 K, 12 Mössbauer absorption lines were observed. These lines are composed of two subspectra, A and B, corresponding to Fe atoms at the 2*a* and 4*i* sites, respectively. At 320 K, the Mössbauer spectrum collapsed, indicating a transition from a ferrimagnetic to a paramagnetic state. This temperature is close to the Curie temperature (T_C) of 331 or 315 K reported in the literature. The analysis of local structural symmetry confirmed that the Fe atoms in the 2*a* sites are more symmetrically coordinated with neighboring Se atoms than those in the 4*i* sites. Therefore, the Fe atoms in the 2*a* sites exhibit a higher hyperfine magnetic field (HMF) of 225 kOe and a weaker quadrupole splitting (QS) of 0.17 mm/s than the Fe atoms in the 4*i* sites, which exhibit an HMF of 105 kOe and a QS of 0.55 mm/s. Our density functional study confirmed that Fe_3Se_4 exhibits ferrimagnetic behavior, with a magnetic moment of 4.48 μ_B/u.c. and a T_C of 354 K. Fe_3Se_4 shows a high magnetocrystalline anisotropy constant (K_u) of 0.9×10^6 erg/cm^3. This high K_u value is attributed to the Fe atoms at the 4*i* sites. It is suggested that the high coercivity of Fe_3Se_4, as reported in the literature, is due to the distorted 4*i* site, which experiences the Jahn–Teller effect.

Index Terms—Magnetism in solids, first-principles calculations, ferrimagnetism, magnetocrystalline energy, Mössbauer spectroscopy.

I. INTRODUCTION

Due to its large magnetocrystalline anisotropy and half-metallic properties, Fe_3Se_4 has the potential to be used in permanent magnets [Zhang 2011, Wang 2012, Shao 2020, Saucedo 2021, Ghalawat 2021], spintronics [Li 2011, Tewari 2020], and superconductors [Chen 2014].

Mössbauer spectroscopy (**MS**) provides insights into hyperfine interactions, local electronic structure, and magnetic fields at a nucleus. This technique involves measuring the transition energies of Fe nuclei using a Mössbauer spectrometer, which utilizes a ^{57}Co source. The ^{57}Co source decays to ^{57}Fe through electron capture, emitting 14.4 keV γ-rays (quanta) that are used to measure the energy. The sample, also known as an absorber, receives the emitted quanta through a collimator. Meanwhile, a proportional counter, known as a detector, detects the transmitted quanta [Hong 1974]. This method is highly effective in characterizing the hyperfine magnetic field (**HMF**) and electric quadrupole splitting (**QS**) (Δ) of Fe-based materials. The magnetic properties of different materials [Jhonson 1996], such as Fe–Pt permanent magnets [Crisan 2020] and soft magnetic materials, such as Fe–Si–Nb–Mo–B–Cu, Fe–Zr–B, Fe–B, and Fe–P–C [Oshima 1979, Greneche 1998, Geneche 2000, Zhu 2019], were investigated using MS. Recently, Alenkina [2022] conducted a comprehensive review of MS applications in nanomaterials, including nanocrystalline soft magnetic materials.

Corresponding authors: Chang-Dong Yeo; Yang-Ki Hong (e-mail: changdong.yeo@ttu.edu; ykhong@eng.ua.edu)
Digital Object Identifier 10.1109/LMAG.2024.3479924

MS detects three types of hyperfine parameters: isomer shift (δ), QS, and HMF. The δ value is closely related to the iron oxidation state, spin state, and bonding properties, as it represents the Coulomb interaction between the protons in the nucleus and the S electrons. The QS value is associated with the interaction between the nuclear quadrupole moment of the ground or excited state and an inhomogeneous electric field at the nucleus. This value is directly connected to the extent of crystal distortion, which determines the magnetocrystalline anisotropy energy (coercivity). The HMF stands for the strength of the magnetic field experienced by a probe nucleus due to its surrounding magnetic moments. This provides valuable information for position assignment and determining magnetic order. It is associated with inequivalent crystallographic sites, such as sublattices. The Curie or Neel temperature (T_C or T_N) of cubic Fe-based materials is determined by the temperature at which a single Mössbauer absorption line is observed.

Pohjonen [2018] used MS to characterize Fe_3Se_4 and reported two different iron sites from the two magnetic sextets observed below the T_C of 331 K. Using temperature-dependent magnetization, a T_C of Fe_3Se_4 was determined to be 315 K [Wang 2012]. Regnard [1971] also reported Mössbauer spectra for Fe_3Se_4, and their analysis revealed a T_C of 320 K.

The origins of ferrimagnetism in Fe_3Se_4, the coexistence of two different magnetic sites, and the high coercivity reported in the literature for Fe_3Se_4 are not fully understood. This study utilized MS and first-principles calculations to elucidate the origins of ferrimagnetism in Fe_3Se_4, encompassing two distinct magnetic sites for Fe: magnetocrystalline anisotropy constant (K_u), and T_C.

II. THEORETICAL

A. Hyperfine Magnetic Field

When the HMF is parallel to the axis of symmetry of the electric field gradient and the electric field is axially symmetric, the Hamiltonian e for the first excited state of Fe^{57} with I = 3/2 can be expressed

$$\mathcal{H}_e = g_1\,\mu_N H I_z + \frac{e^2qQ}{12}\left(3I_z^2 - \frac{15}{4}\right)$$

which is diagonal in the basis $|3/2m\rangle$. Accordingly, the diagonal elements of the 4 × 4 magnetic hyperfine and quadrupole interaction matrix are as follows [Ok 1968]:

$$\left\langle \frac{3}{2}\frac{3}{2}\right| \mathcal{H}_e \left|\frac{3}{2}\frac{3}{2}\right\rangle = \frac{3}{2}\,g_1\mu_N H + \frac{e^2qQ}{4} \tag{1}$$

$$\left\langle \frac{3}{2}\frac{1}{2}\right| \mathcal{H}_e \left|\frac{3}{2}\frac{1}{2}\right\rangle = \frac{1}{2}\,g_1\mu_N H - \frac{e^2qQ}{4} \tag{2}$$

$$\left\langle \frac{3}{2}\frac{-1}{2}\right| \mathcal{H}_e \left|\frac{3}{2}\frac{-1}{2}\right\rangle = -\frac{1}{2}g_1\mu_N H - \frac{e^2qQ}{4} \tag{3}$$

$$\left\langle \frac{3}{2}\frac{-3}{2}\right| \mathcal{H}_e \left|\frac{3}{2}\frac{-3}{2}\right\rangle = -\frac{3}{2}g_1\mu_N H + \frac{e^2qQ}{4}. \tag{4}$$

Six gamma-ray transitions between the first excited state and the ground state of Fe^{57} of pure M1 type have the following energy splitting [Ok 1971]:

$$E_1 = \frac{(3g_1 + g_0)}{2}\,\mu_N H + \frac{e^2qQ}{4} \tag{5}$$

$$E_2 = \frac{(g_1 + g_0)}{2}\,\mu_N H - \frac{e^2qQ}{4} \tag{6}$$

$$E_3 = \frac{(-g_1 + g_0)}{2}\,\mu_N H - \frac{e^2qQ}{4} \tag{7}$$

$$E_4 = \frac{(g_1 - g_0)}{2}\,\mu_N H - \frac{e^2qQ}{4} \tag{8}$$

$$E_5 = \frac{(-g_1 - g_0)}{2}\,\mu_N H - \frac{e^2qQ}{4} \tag{9}$$

$$E_6 = \frac{(-3g_1 - g_0)}{2}\,\mu_N H + \frac{e^2qQ}{4}. \tag{10}$$

To calculate the transition probabilities between the four nondegenerate levels corresponding to the excited state and the two corresponding to the ground state, we must consider the angle (θ) between the magnetic field and the incident gamma-ray direction. The relative transition probabilities for a 3/2 to 1/2 transition are determined by the Clebsch–Gordon coefficients. Therefore, the intensities for the six transitions can be expressed as [Preston 1962]

- $I_{1,6} = 3\,(1 + \cos^2\theta)$ for ± 2/3 → ± 1/2 transition;
- $I_{2,5} = 4\,\sin^2\theta$ for ± 1/2 → ± 1/2 transition;
- $I_{3,4} = 1 + \cos^2\theta$ for ± 1/2 → ∓ 1/2 transition.

A single iron crystal holds six absorption peaks in a Mössbauer spectrum. However, the relative intensities of these peaks change and become 3 : 2 : 1 : 1 : 2 : 3 for a powder sample. In addition, for a well-defined crystalline sample, the angle θ schematically shown in Fig. 1 can be determined by the intensity ratio of peak 2 to 3 using the following:

$$\theta = \arcsin\sqrt{\frac{2}{1 + \frac{4}{I_{23}}}}. \tag{11}$$

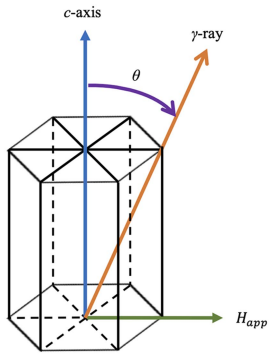

Fig. 1. Definition of theta (θ).

By performing a quantitative analysis of the relative intensities and absorption line peaks mentioned above, one can obtain essential information about the magnetism of Fe_3Se_4. This information includes δ, Δ (or QS), HMF, T_C, and magnetic Fe sites. The Mössbauer spectrum was analyzed using a nonlinear least squares computer fitting program, assuming the Lorentzian function describes all peak shapes. A detailed analysis can be found in Hong [1974].

B. First-Principles Calculations of Electronic Structures

The WIEN2k package employs density functional theory (**DFT**) using the local spin density approximation (**LSDA**) and the full potential linearized augmented plane wave method for first-principles calculations [Blaha 2001]. To calculate electronic structures and density of states, all calculations used a 19 × 19 × 27 k-point mesh, generating 1400 k-points in the irreducible part of the Brillouin zone. The first-principles calculations for monoclinic Fe_3Se_4 used the following lattice constants: a = 6.16 Å, b = 3.53 Å, and c = 11.1 Å. This calculation employs 16 valence electrons for Fe ($3s^23p^63d^64s^2$) and six valence electrons for Se ($4s^24p^4$).

Magnetocrystalline anisotropy energy ($\Delta E_{MAE} = E\langle 100\rangle - E\langle 001\rangle$) is calculated using the following:

$$\Delta E_{MAE} = \sum_i \varepsilon_i(\hat{n}_1) - \sum_i \varepsilon_i(\hat{n}_2) = E^{\text{total}}(\hat{n}_1) - E^{\text{total}}(\hat{n}_2) \tag{12}$$

where $\hat{n}_1$ and $\hat{n}_2$ are easy and hard spin directions, respectively. Regarding T_C calculation, the exchange integrals (J_{0j}) were calculated using the energy difference between the ground and excited states. The exchange integrals (J_{0j}) consider interactions over all neighboring spins, then $J_0 = \sum_j J_{0j}$ [Novak 2005]. The T_C is calculated with J_0 using the following mean-field approximation [MacLaren 1999]:

$$T_C = \frac{2}{3k_B}\,J_0\gamma \tag{13}$$

where J_0 is the molecular field parameter calculated by summing the exchange integrals J_{0j} and k_B is the Boltzmann constant. The factor γ equals $S(S+1)/S^2$, where S is the spin angular momentum.

III. EXPERIMENTAL

To start the synthetic process, an empty quartz tube measuring 1 cm in diameter and 5 cm in length was heated at 800 °C in an H_2 stream to eliminate any traces of oxygen. Then, a mixture of natural iron, enriched iron, and selenium powders was loaded into the reduced

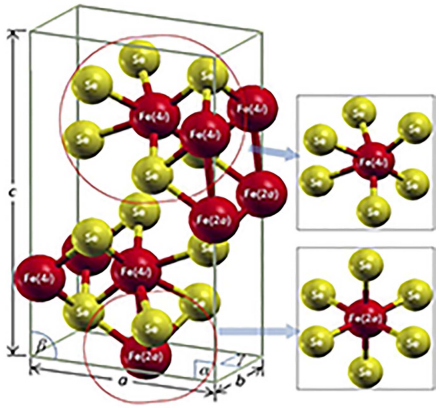

Fig. 2. Crystal structure of monoclinic Fe_3Se_4, showing two different atomic coordination.

Table 1. Relative energy versus different magnetization direction for Fe_3Se_4.

	<100>	<010>	<001>	<110>
Relative E_{tot} in mRy	-0.038	-0.144	0.000	-0.032
(10^{-23}J)	(-8.284)	(-31.39)		(-6.976)

quartz tube before being evacuated and sealed in a vacuum. The sealed tube was then placed inside another heating quartz tube, which measures 2 cm in diameter and 50 cm in length.

The doubled tube was heated in a high-purity nitrogen gas stream to 600 °C for 12 h. The temperature was then raised to 900 °C and kept for 6 h, then heated to 1100 °C for 1 h. The tube was held at 950 °C for two days and decreased to 400 °C at a 550 °C/h rate. The tube was then quenched to room temperature, and the resulting Fe_3Se_4 sample was ground into powder. Two Fe_3Se_4 powder samples were prepared. One sample was used for X-ray diffraction analyses. At the same time, the other was sandwiched between beryllium plates (0.127 mm thick) to prevent oxidation, resist high temperatures, and facilitate the passage of gamma rays for Mössbauer measurement.

Mössbauer spectra were obtained by a constant acceleration Mössbauer spectrometer of the electromechanical drive type with a loudspeaker [Ok 1972].

IV. RESULTS AND DISCUSSION

Fig. 2 illustrates the crystal structure of monoclinic Fe_3Se_4, focusing on the 2*a* and 4*i* sublattices. The equilibrium lattice constants of the Fe_3Se_4 system were obtained by relaxing the system, resulting in the values of $a = 6.16$ Å, $b = 3.53$ Å, and $c = 11.1$ Å. These values agreed with the corresponding theoretical [Long 2011] and experimental constants [Singh 2020]. These lattice parameters were used in our first-principles calculations.

We performed first-principles calculations to determine the relative total energy (E_{tot}) for ferromagnetic and ferrimagnetic Fe_3Se_4 systems. The results show that the ferrimagnetic structure is more stable than the ferromagnetic one, with a relative E_{tot} of −13.468 mRy (or -2.936×10^{-20} J) compared to the ferromagnetic system. In addition, we calculated the total energy of Fe_3Se_4 along four different magnetization directions, and the results are listed in Table 1.

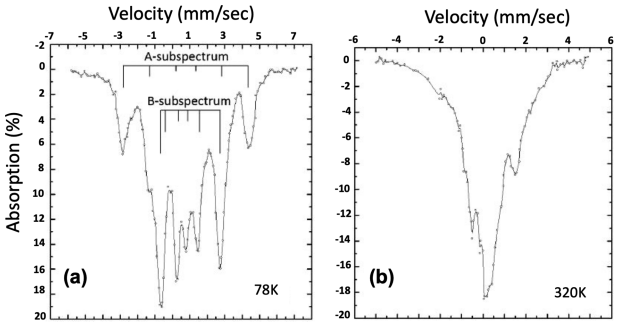

Fig. 3. Mössbauer spectra at (a) 78 K and (b) 320 K [Hong 1974].

Table 2. Mössbauer parameters: MHF and QS at 78 K.

	Hyperfine magnetic field (kOe)	Quadrupole spilling (mm/sec)
A-subspectrum [Fe(2*a*)]	225	0.17
B-subspectrum [Fe(4*i*)]	105.5	0.55

The preferred direction of magnetization with the lowest energy is aligned along the <010> axis. Using (12), the magnetocrystalline anisotropy energy, $\Delta E = E_{001} - E_{010}$, was calculated to be 1.444 meV/u.c. The calculated K_u is 0.9×10^6 erg/cm^3, approximately one order of magnitude smaller than the 6×10^6 erg/cm^3 reported by Zhang [2011]. This high K_u of Fe_3Se_4 is attributed to its high coercivity, as reported in the literature.

The synthesized Fe_3Se4 powder samples were characterized by X-ray diffraction and found to have a monoclinic crystal structure. The X-ray diffraction pattern is not shown here.

Fig. 3 shows the Mössbauer spectra measured at 78 and 320 K. The spectrum at 78 K comprises two distinct sextet spectra, corresponding to A and B subspectra for 2*a* and 4*i* sites, respectively. Noticeably, the absorption lines are closely spaced in the B subspectrum, indicating larger QS than the A-spectrum. The appearance of two sextet absorption lines at 78 K confirms the two magnetic sites for Fe. As the temperature rises, the separation between the absorption lines reduces gradually. At 320 K, the 12 absorption lines merge into a pseudosingle line or collapse. It seems like there might be a magnetic transition from a ferrimagnetic to a paramagnetic state at a temperature near or higher than 320 K. This temperature is close to the T_C of 331 K in Li [2015] and Pohjonen [2018], as well as the 315 K in Wang [2012]. The T_C can be determined experimentally using the temperature-dependent HMF [Morais 1983].

Mössbauer parameters encompass HMF, QS, and isomer shift (**IS**) derived from the measured Mössbauer spectra. The absorption peak positions (v_i) and spacing of a sextet spectrum are used to determine Mössbauer parameters: IS $= (v_1 + v_2 + v_5 + v_6)/2$ (mm/s) for the balance state of Fe; QS $= 1/2[(v_1 - v_2) - (v_5 - v_6)]$ (mm/s) for structure distortion (magnetocrystalline anisotropy); HMF $= 31.047\ (v_1 - v_6)$ for spin canting and magnetic ordering (structure). The Mössbauer parameters obtained from the spectrum analysis of Fig. 3(a) are listed in Table 2.

As shown in Table 2, HMF is higher at the 2*a* site than at the 4*i* site. On the other hand, the QS at the 4*i* site is stronger than the 0.17 mm/s at

Table 3. Calculated magnetic moments per formula unit from (a) LSDA and (b) GGA potential.

(a) LSDA	Spin Moment (μ_B)			Orbital Moment (μ_B)			Total Moment in $\mu_B/f.u.$
	Fe(2*a*)	Fe(4*i*)	Se	Fe(2*a*)	Fe(4*i*)	Se	(10^{-24} J/T)
Spin-polarized	-2.15	2.06	-0.0003	-	-	-	1.96 (18.18)
<010>	-2.12	2.05	-0.0046	-0.09727	0.07415	-0.00017	2.01 (18.64)
(b) GGA	Spin Moment (μ_B)			Orbital Moment (μ_B)			Total Moment in $\mu_B/f.u.$
	Fe(2*a*)	Fe(4*i*)	Se	Fe(2*a*)	Fe(4*i*)	Se	(10^{-24} J/T)
Spin-polarized	-2.34	2.27	-0.0003	-	-	-	1.96 (18.18)
<010>	-2.35	2.27	-0.0003	-0.08614	0.06818	-0.0002	2.23 (20.68)

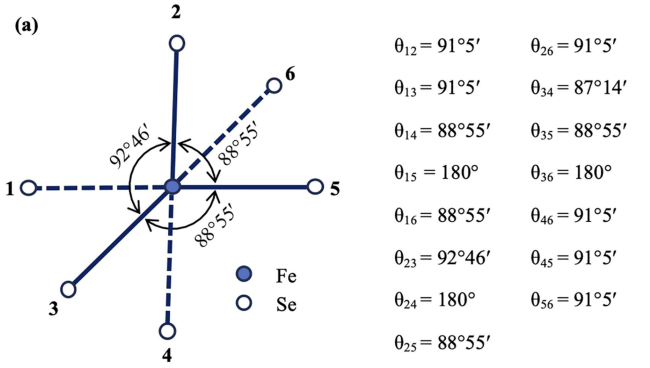

The Local symmetry of Fe ion at 2*a* site in Fe_3Se_4

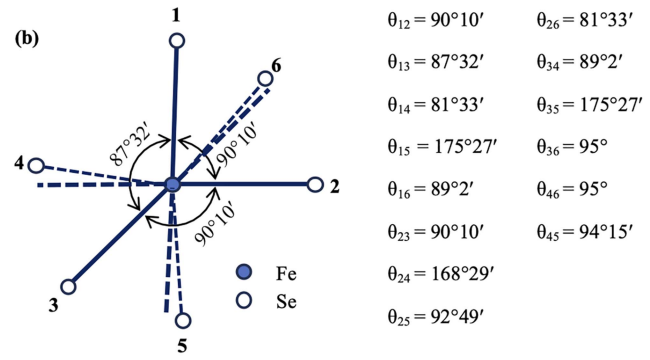

The Local symmetry of Fe ion at 4*i* site in Fe_3Se_4

Fig. 4. Local symmetry of Fe (a) at 2*a* and (b) 4*i* sites in Fe_3Se_4.

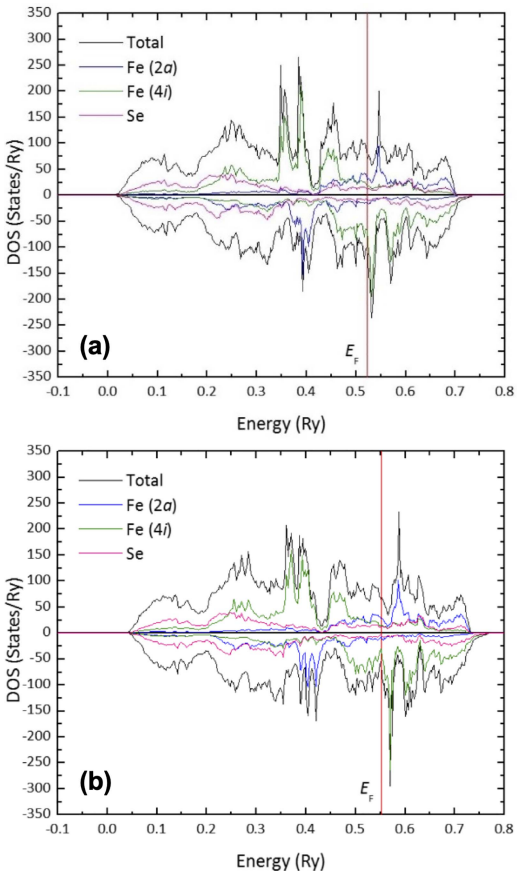

Fig. 5. Density of states for Fe_3Se_4. (a) LSDA. (b) GGA results.

the 2*a* site. These findings align with the results of the first-principles calculation in Table 3, indicating a higher HMF for the 2*a* site.

The difference in the QS of the 2*a* and 4*i* sites can be understood by the local symmetry of the Fe site in Fig. 4. Local atomic coordination for the 4*i* site is more distorted than for the 2*a* site. Six Fe atoms in the monoclinic formula unit (f.u.) occupy two 2*a* and 4*i* sites. In the 2*a* site, Fe has nearly perfect octahedral coordination with six neighboring Se, as shown in Fig. 4(a). In contrast, Fe in the 4*i* site has less symmetric coordination, i.e., crystal structure distortion, for neighboring Se atoms, as shown in Fig. 4(b), demonstrating that the QS for the 4*i* Fe site is greater than the 2*a* site. These results confirm that A and B subspectra originate from Fe in 2*a* and 4*i* sites, respectively.

The theoretical method described in Section II was used to calculate the electronic structures of Fe_3Se_4 to support Mössbauer HMF results and ferrimagnetism. Fig. 5(a) and (b) shows the density of states for Fe_3Se_4 obtained from LSDA and generalized gradient approximation (**GGA**) potential, respectively. The calculated density of states (**DOS**) agrees with the DOS reported by Islam [2023], and the corresponding magnetic moments are listed in Table 3. Regardless of LSDA or GGA methods, the Fe atom at the 2*a* sites contributes more to spin polarization than at the 4*i* sites, and the spin direction at the 2*a* sites is opposite to the 4*i* sites, as seen in Table 3, confirming the ferrimagnetism of Fe_3Se_4. The Fe_3Se_4 f.u. contains one Fe atom at the 2*a* site and two Fe atoms at the 4*i* sites, and its unit cell has two and four Fe atoms, respectively. The total moment per Fe_3Se_4 f.u. is 2.23 μB for <010> direction under GGA, leading to 4.48 μB/u.c. (unit cell) in reasonable agreement with 4.25 μB/u.c. in Singh [2020] and 4.29 μB/u.c. in Yadav [2022]. Two Fe sites were confirmed by the two sub-Mössbauer spectra at 78 K and explained by the density of states.

Next, to calculate T_C, we identified the number of the nearest neighboring atoms and the distance between the atoms, as shown in Table 4. Then, the exchange integral (J_{0j}) was calculated for the exchange energy, followed by calculating T_C using (13). The calculated

Table 4. Fundamental parameters for the calculation of Curie temperature.

	# of nearest neighbors			Distances (Å)		
Fe_3Se_4	1	1	1	2.89	3.00	2.88

Exchange integrals	J_{01} (meV)	J_{02} (meV)	J_{03} (meV)
	7.44	12.57	12.73

T_C is 354 K, which is close to 331 K in Li [2015] and 315 K in Wang [2012].

The presence of two different Fe sites was confirmed by analyzing the two sub-Mössbauer spectra measured at 78 K. The difference in the QS between the Fe sites at 2*a* and 4*i* was attributed to the local symmetry of Fe at these sites. The DFT study confirms that the magnetic spin of Fe at the 2*a* site is opposite to that of the 4*i* site, which leads to ferrimagnetism. The high coercivity of Fe_3Se_4 was explained through the calculation of magnetocrystalline anisotropy energy, which measures how strongly a material's coercivity depends on its crystal orientation.

V. CONCLUSION

MS determined that two separate magnetic sites, 2*a* and 4*i*, are present in Fe_3Se_4. Fe atoms at the 2*a* site have a higher HMF of 225 kOe and a weaker QS of 0.17 mm/s than Fe atoms at the 4*i* site, having a hyperfine magnetic field of 105 kOe and a QS of 0.55 mm/s. This is because the Fe atoms at the 2*a* site are symmetrically coordinated with their neighboring Se atoms, while those at the 4*i* site are not. The DFT study results show a T_C of 354 K and confirm that Fe_3Se_4 is ferrimagnetic. The high magnetocrystalline anisotropy (0.9×10^6 erg/cm^3) of Fe_3Se_4 is attributed to the less symmetric coordination of the Fe atom at the 4*i* site with its six neighboring Se atoms. This explains the high coercivity of Fe_3Se_4 found in the literature as well.

ACKNOWLEDGMENT

This work was supported in part by the National Science Foundation under Grant 2137275 and in part by the E. A. "Larry" Drummond Endowment, University of Alabama.

REFERENCES

Alenkina IV, Ushakov MV, Morais PC, Kalai S R, Kuzmann E, Klencsár Z, Felner I, Homonnay Z, Oshtrakh MI (2022), "Mössbauer spectroscopy with a high velocity resolution in the studies of nanomaterials," *Nanomaterials*, vol. 12, 3748, doi: 10.3390/nano12213748.

Blaha P, Schwarz K, Madsen G K H, Kvasnicka D, Luitz J, Laskowsk R, Tran F, Marks L (2001), *WIEN2K: An Augmented Plane Wave + Local Orbitals Program for Calculating Crystal Properties*. Wien, Austria: Karlheinz Schwarz, Techn. Universitat.

Chen T K, Chang C C, Chang H H, Fang A H, Wang C H, Chao W H, Tseng C M, Lee Y C, Wu Y R, Wen M H, Tang H Y, Chen F R, Wang M J, Wu M K, and Van Dyck D (2014), "Fe-vacancy order and superconductivity in tetragonal β-Fe1-xSe," *Proc. Nat. Acad. Sci.*, vol. 111, pp. 63–68, doi: 10.1073/pnas.1321160111.

Crisan O, Dan I, Palade P, Crisan A D, Leca A, Pantelica A (2020), "Magnetic phase coexistence and hard-soft exchange coupling in FePt nanocomposite magnets," *Nanomaterials*, vol. 10, 1618, doi: 10.3390/nano10081618.

Genèche J M, Miglierini M, Slawska-Waniewska A (2000), "Iron-based nanocrystalline alloys investigated by ^{57}Fe Mössbauer spectrometer," *Hyperfine Interact.*, vol. 126, pp. 27–34, doi: 10.1023/A:1012663921858.

Ghalawat M, Podda P (2021), "Study of growth kinetics of Fe_3Se_4 nanocrystallites and the influence of size and shape tunability on their magnetic properties," *J. Phys. Chem. C*, vol. 125, pp. 7932–7943, doi: 10.1021/acs.jpcc.1c00389.

Greneche J M, Randrianantoandro N, Slawska-Waniewska A, Miglierini M (1998), "Magnetic hyperfine properties in FeZrB-type nanocrystalline metallic alloys," *Hyperfine Interact.*, vol. 113, pp. 279–285, doi: 10.1023/A:1012636019055.

Hong Y K (1974), "Mössbauer study of ferrimagnetic Fe_3Se_4," M.S. thesis, Dept. Phys., Yonsei Univ., Seoul, South Korea.

Islam R, Borah J P (2023), "3*d* transition metal substituted Fe_3Se_4: Prediction of potential permanent magnet," *J. Phys.: Condens. Matter*, vol. 35, 325801, doi: 10.1088/1361-648X/acd319.

Johnson C E (1996), "Characterization of magnetic materials by Mössbauer spectroscopy," *J. Phys. D: Appl. Phys.*, vol. 29, 2266, doi: 10.1088/0022-3727/29/9/007.

Li D, Jiang J J, Liu W, Zhang Z D (2011), "Positive magnetoresistance in Fe_3Se_4 nanowires," *J. Appl. Phys.*, vol. 109, 07C705, doi: 10.1063/1.3544508.

Li S, Li D, Liu W, Zhang Z (2015), "High Curie temperature and coercivity performance of $Fe_{3-x}Cr_xSe_4$ nanostructures," *Nanoscale*, vol. 7, pp. 5395–5402.

Long G, Zhang H, Li D, Sabirianov R, Zhang Z, Zeng H (2011), "Magnetic anisotropy and coercivity of Fe_3Se_4 nanostructures," *Appl. Phys. Lett.*, vol. 99, 202103, doi: 10.1063/1.3662388.

MacLaren J M, Schulthess T C, Butler W H, Sutton R, McHenry M (1999), "First principles study on the electronic structure and effective exchange interaction of $Y(Co_{1-x}Cu_x)_5$," *J. Appl. Phys.*, vol. 85, 4833, doi: 10.1063/1.2176316.

Morais P C, Neto K S (1983), "Study of magnetism in fine particles of ferric hydroxysulfate by Mössbauer spectroscopy," *J. Appl. Phys.*, vol. 54, pp. 307–314, doi: 10.1063/1.331702.

Novák P, Rusz J (2005), "Exchange interactions in barium hexaferrite," *Phys. Rev. B*, vol. 71, 184433, doi: 10.1103/PhysRevB.71.184433.

Ok H N (1971), "A study on the magnetic hyperfine field at Fe_{57} in permalloy," *New Phys.*, vol. 11, 49. [Online]. Available: https://www.npsm-kps.org/journal/view.html?uid=4418

Ok H N, Lee S W, Cho Y C (1972), "Constant acceleration Mössbauer spectrometer," *New Phys.*, vol. 12, 142. [Online]. Available: https://www.npsm-kps.org/journal/view.html?uid=4364

Ok H N, Mullen J G (1968), "Magnetic properties of iron ions in CoO(I) and CoO(II)," *Phys. Rev.*, vol. 168, 563, doi: 10.1103/PhysRev.168.563.

Oshima R, Fujita F E, Fukamichi K, Masumoto T (1979), "Mössbauer spectroscopy of amorphous Fe-B alloys," *J. Phys. Colloques*, vol. 40, pp. C2-132–C2-134, doi: 10.1051/jphyscol:1979245.

Pohjonen R, Mustonen O, Karppinen M, LindénJ (2018), "Mössbauer study of magnetism in Fe_3Se_4," *J. Alloys Compounds*, vol. 746, pp. 135–139, doi: 10.1016/j.jallcom.2018.02.257.

Preston R S, Hanna S S, Heberle J (1962), "Mössbauer effect in metallic iron," *Phys. Rev.*, vol. 128, 2207, doi: 10.1103/PhysRev.128.2207.

Regnard J R, Hocquenghem J C (1971), "Étude par effet Mössbauer du composé semi-métallique a ordre lacunaire Fe_3Se_4," *J. Phys. Colloq.*, vol. 32, pp. C1-268–C1-270, doi: 10.1051/jphyscol:1971189.

Saucedo L A, Clark J K, Winfred J R S V, Strouse G F, Shatruk M (2021), "Increasing magnetic hardness of Fe_3Se_4 via Cu doping," *J. Phys. Chem. C*, vol. 125, pp. 25784–25793, doi: 10.1021/acs.jpcc.1c06841.

Shao Z, Ren S (2020), "Rare-Earth-free magnetically hard ferrous materials," *Nanoscale Adv.*, vol. 2, pp. 4341–4349, doi: 10.1039/D0NA00519C.

Singh D, Gupta S K, He H, Sonvane Y (2020), "First-principles study of the electronic, magnetic and optical properties of Fe_3Se_4," *J. Magn. Magn. Mater.*, vol. 498, 16615720, doi: 10.1016/j.jmmm.2019.166157.

Tewari G C, Srivastava D, Pohjonen R, Mustonen O, Karttunen A J, Lindén J, and Karppinen M (2020), "Fe_3Se_4: A possible ferrimagnetic half-metal?," *J. Phys.: Condens. Matter*, vol. 32, 455801, doi: 10.1088/1361-648X/aba3ef.

Wang J, Duan H, Lin X, Aguilar V, Mosqueda A (2012), "Temperature dependence of magnetic anisotropy constant in iron chalcogenide Fe_3Se_4," *J. Appl. Phys.*, vol. 112, 103905, doi: 10.1063/1.4759352.

Yadav S J, Jasani J, Kumavat S R, Singh D, Shah D V, Sonvane Y, Ahuja R (2022), "Tuning the electronic and magnetic properties of Fe_3Se_4 material by mechanical strain," *Materials Int.*, vol. 4, 2, doi: 10.33263/Materials41.002.

Zhang H, Long G, Li D, Sabirianov R, Zeng H (2011)," Fe_3Se_4 nanostructures with giant coercivity synthesized by solution chemistry," *Chem. Mater.*, vol. 23, pp. 3769–3774, doi: 10.1021/cm201610k.

Zhu L, Meng Y, Zhai X B, Wang Y G, Lan S (2019), "Structure origin of abnormal magnetic behavior of Fe-PC amorphous alloys," *J. Magn. Magn. Mater.*, vol. 472, pp. 49–52, doi: 10.1016/j.jmmm.2018.10.001.